Acta Biomaterialia 91 (2019) 48–59

Contents lists available at ScienceDirect

Acta Biomaterialia

journal homepage: www.elsevier.com/locate/actabiomat

Full length article

In vivo and *in vitro* bioactivity of a "precursor of apatite" treatment on polyetheretherketone

Kazutaka Masamoto [a,*], Shunsuke Fujibayashi [a], Takeshi Yabutsuka [b], Tomoko Hiruta [b], Bungo Otsuki [a], Yaichiro Okuzu [a], Koji Goto [a], Takayoshi Shimizu [a], Yu Shimizu [a], Chihiro Ishizaki [b], Keito Fukushima [b], Toshiyuki Kawai [a], Makoto Hayashi [a], Kazuaki Morizane [a], Tomotoshi Kawata [a], Masashi Imamura [a], Shuichi Matsuda [a]

[a] Department of Orthopaedic Surgery, Kyoto University Graduate School of Medicine, Kyoto, Japan
[b] Department of Fundamental Energy Science, Graduate School of Energy Science, Kyoto University, Kyoto, Japan

ARTICLE INFO

Article history:
Received 5 December 2018
Received in revised form 20 March 2019
Accepted 17 April 2019
Available online 19 April 2019

Keywords:
PEEK
Bioactivity
Precursor of apatite (PrA)
Pore formation
Oxygen plasma treatment
H_2SO_4

ABSTRACT

We recently developed a surface treatment, "precursor of apatite" (PrA), for polyetheretherketone (PrA-PEEK) via a simple, low-temperature process aiming to achieve stronger and faster adhesion to bone. The treatment involves three steps: H_2SO_4 immersion, exposure to O_2 plasma discharge, and alkaline simulated body fluid (alkaline SBF) treatment. This method produces homogeneous fine particles of amorphous calcium phosphate on the PEEK, and we confirmed that PrA-PEEK had excellent apatite formation ability in an SBF immersion test. In the present study using PEEK implants in rabbit tibia, mechanical tests, and histological and radiological analyses revealed that PrA provided the PEEK substrate with excellent bone-bonding properties and osteo-conductivity at early stages (4 and 8 weeks), extending to 16 weeks. *In vitro* study using MC3T3-E1 cells revealed via XTT assay that PrA on the PEEK substrate resulted in no cytotoxicity, though PrA treatment seemed to suppress gene expression of *integrin β-1* and *Alp* after 7-day incubation as shown by real-time PCR. On the whole, PrA treatment succeeded in giving *in vivo* bone-bonding properties to the PEEK substrate, and the treatment is a safe and promising method that can be applied in clinical settings. There was an inconsistency between *in vivo* and *in vitro* bioactivity, and this discrepancy indicated that apatite formation does not always need activation of osteoblasts at very early stage and that optimal conditions at cell and organism level may be different.

Statement of Significance

Polyetheretherketone (PEEK) is an attractive engineering polymer used for spine and dental surgery. To further improve clinical outcome of PEEK-based materials, we developed "Precursor of apatite" (PrA) treatment on the PEEK surface to confer bone-bonding properties. The advantages of this treatment are that it does not require high-temperature processing or special chemicals, and it is inexpensive. The present study clarified excellent *in vivo* bone-bonding property of PrA treatment. In addition, the results revealed important insights indicating that optimal conditions, especially wettability and crystallinity in calcium phosphate, differ at cell and organism levels. Moreover, our results indicated that prediction of *in vivo* bioactivity should be done in combination with multiple *in vitro* tests.

1. Introduction

Polyetheretherketone (PEEK) is an attractive engineering polymers for medical applications, with advantages such as low elastic modulus similar to that of cortical bone, radiolucency, and resistance to fatigue, chemicals, and shock [1]. PEEK has already been widely used in spine and dental surgery, and PEEK implants generally show satisfactory results in clinical applications. In a meta-analysis, Seaman et al. investigated the clinical outcomes of spinal fusion surgery using PEEK or titanium implants and reported that PEEK cage had a statistically similar fusion rate and a lower subsidence rate than titanium cage [2]. The beneficial clinical outcomes

* Corresponding author at: Department of Orthopaedic Surgery, Graduate School of Medicine, Kyoto University, 54 Shogoin Kawahara-cho, Sakyo-ku, Kyoto 606-8507, Japan.
E-mail address: masamoto@kuhp.kyoto-u.ac.jp (K. Masamoto).

https://doi.org/10.1016/j.actbio.2019.04.041
1742-7061/

seen with PEEK implants are considered to be associated with its mechanical properties mentioned above.

Another important feature of PEEK is bio-inertness, meaning that it induces hardly any interaction with a living body [3]. In clinical applications this characteristic is, on the one hand, a great advantage, but on the other is its biggest drawback. In fact, this bio-inertness, along with progress in surgical techniques, has promoted the application of PEEK implants, but equally has raised another problem, pseudoarthrosis, especially when PEEK implants are used in elderly people. In surgery on this section of the population, bone vulnerability is a matter of concern (especially the accomplishment of bone fusion), and the raised incidence of osteoporosis increases the risk of failure in spinal fusion surgery [4]. Therefore, it is necessary to confer bioactive properties, especially bone-bonding properties, on PEEK in order to further improve surgical success rates. Moreover, cost reductions for this kind of treatment should be sought in an era of soaring medical costs.

There have already been many reports on treatment methods for improving the bioactivity of PEEK. The reported methods can be divided into composites and surface treatment [5]. Examples of components of composites include hydroxyapatite [6,7], fluorohydroxyapatite [8], Sr-containing hydroxyapatite [9], β-TCP [10], TiO_2 [11], and CaO-SiO_2 [12]. Surface treatments include chemical deposition (—ONa, —OH, —F, etc.) [13], plasma treatment (O_2 [14], NH_3 [15], Ar [14], N_2 [16], etc.), deposition of bioactive materials (hydroxyapatite [17], TiO_2 [18], and gelatin with BMP2 [19]. However, there are unsolved problems associated with the existing treatment methods; they often require high-temperatures, complicated procedures or special apparatus and chemicals, and they are costly.

To overcome these problems, we recently developed a surface treatment of PEEK called "precursor of apatite" (PrA), which produces a homogeneous layer of fine particles of amorphous calcium phosphate (ACP) on the PEEK surface [20]. The concept of this treatment is "stronger and faster adhesion to bone with a simple low-temperature procedure," and the technique comprises three steps: immersion in H_2SO_4, O_2 plasma treatment, and alkaline simulated body fluid (alkaline SBF) treatment. We revealed that this treatment resulted in excellent apatite formation in SBF (ISO 23317 [21]) and that the first and the second steps were crucial for consolidating the adhesion strength between the PrA-treated PEEK (PrA-PEEK) substrate and the apatite layer newly-formed in SBF. On achieving these results, we evaluated the bioactivity and safety of PrA for clinical application. The goal of the present study was to evaluate the effect of PrA treatment on *in vivo* bone-bonding strength and on *in vitro* cell compatibility and differentiation.

2. Materials and methods

2.1. PEEK implants fabrication

2.1.1. PEEK sample preparation

Commercial PEEK (Ketron® 1000 PEEK, Quadrant Polypenco Japan, Japan) was shaped either into a plate format (15 × 10 × 2 mm) for *in vivo* study or a disk format (18 mm diameter × 2 mm) for analyses of surface characteristics and *in vitro* study (Fig. 1A(a)). Both substrate types were washed, in order, with 99.5% acetone, 99.5% ethanol, and distilled water in an ultrasonic cleaner for 10 min and air dried at room temperature.

2.1.2. Treatment methods of PrA treatment and four groups of PEEK

Treatment methods of PrA were described in our previous report [20]. First, to create surface pores 500 nm in diameter (step S), PEEK substrates were soaked in 98 wt% H_2SO_4 (Hayashi Pure Chemical., Ltd., Osaka., Japan) for 2 s twice, washed with distilled water, and air dried at room temperature. Next, the samples were exposed to glow discharge in an O_2 atmosphere at 200 W (Kyoto Teisan K.K., Kyoto, Japan) for 4 min to make the surface hydrophilic (step P). Finally, the substrates were immersed in alkaline SBF, in which the pH was increased to 8.4 by dissolving tris (hydroxymethyl) aminomethane at 25 °C, and maintained at 70 °C for 24 h in an incubator to deposit PrA on the PEEK surface (step A). SBF was prepared according to the past report [22]. The changes on PEEK surface given by each step observed by SEM and EDX, together with the result of SBF immersion test using PrA-PEEK, are summarized in Fig. 1B [20,23]. In the present study, four groups of PEEK samples were prepared. For the first group the substrates were washed only with acetone, ethanol, and distilled water, and then dried (group N). Substrates in the second group were additionally treated with H_2SO_4 (group S). Substrates in the third group were treated with H_2SO_4 (step S) and O_2 glow discharge (step P) but not immersion in alkaline SBF (group SP). Substrates in the last group were treated with all the three steps mentioned above (group SPA). For the analyses of surface characteristics, groups N, S, SP, and SPA were tested. For the *in vitro* study, groups N, SP, and SPA were evaluated. For the *in vivo* study, groups N and SPA were investigated to evaluate bioactivity of PrA. All the samples were sterilized with ethylene oxide gas (ekitekku95, Nihon Ekitan, Tokyo, Japan) at a temperature of 40 °C before use in the experiments.

2.2. Surface characteristics

2.2.1. X-ray photoelectron spectroscopy (XPS)

The elemental composition and functional groups on each PEEK substrate were analyzed by XPS (JPS-9010TRX, JEOL Ltd, Japan) using Mg-Kα radiation at an acceleration voltage of 10 kV.

2.2.2. Hydrophilicity, Ca/P ratio, and thickness of PrA

The hydrophilicity of each group of PEEK was evaluated by water contact angle (WCA) using five PEEK samples for each group. The contact angle was measured using Sessile drop method by means of contact angle meter (CAX-150, Kyowa Interface Science, Inc, Japan). One-μL ultrapure water at 25 °C was dropped onto each PEEK surface, and WCA was measured 1 s after the drop.

The Ca/P ratio of PrA was evaluated as follows: The disk-shaped PEEK substrate of group SPA was soaked in 1 M HNO_3 (FUJIFILM Wako Pure Chemical Corporation, Japan) for 24 h at room temperature, and PrA on PEEK substrate was dissolved into the solution. The concentration of Ca and P was evaluated with inductively coupled plasma atomic emission spectroscopy (ICP-AES, ICPS-7510, SHIMADZU CORPORATION, Japan). Following that, the Ca/P ratio was calculated using three samples of group SPA.

The thickness of PrA was evaluated as follows: The disk-shaped PEEK of group SPA was embedded in epoxy resin, and the specimen was cut with diamond wheel (Model 650, South Bay Technology Inc.). Subsequently, the interface between the PEEK substrate and the resin was observed by SEM (SU6600, Hitachi Technologies and Services, Ltd., Japan) with color mapping by EDX (XFlash® 5010, Bruker). The thickness of PrA was estimated based on the depth of the colored area.

2.3. In vitro study

A MC3T3-E1 cell line, as representative of pre-osteoblast cells, was used for all *in vitro* studies. α-MEM (Gibco, USA) with 10% fetal bovine serum and 1% penicillin/streptomycin was used for cell culture in all experiments, and the medium was changed every other day. In all the *in vitro* studies, first, MC3T3-E1 cells were seeded on the disk-shaped PEEK substrate at densities of 1×10^4 cells/cm^2 in 12-well plates and incubated at 37 °C. Four or five PEEK disks were

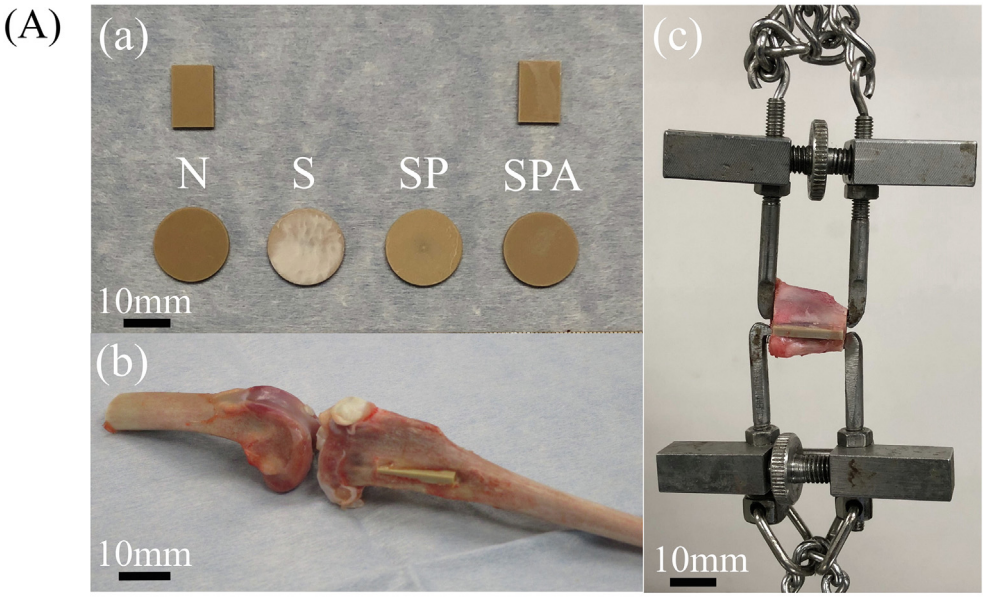

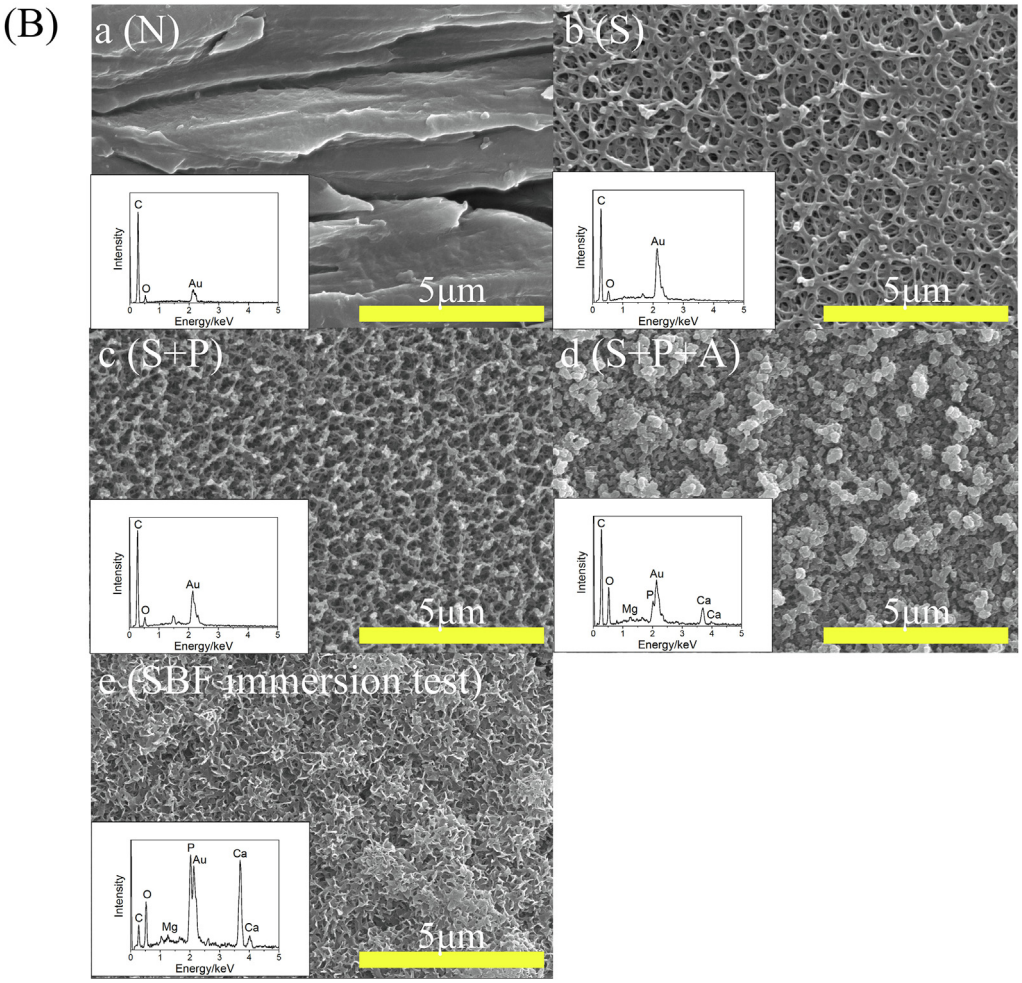

Fig. 1. (A): a, A photo of four groups of PEEK substrate. b, Either group N or SPA PEEK substrate was implanted in the slit in a press-fit manner. c, An apparatus used in the mechanical test. (B): The surface characteristics of PEEK substrate observed by SEM and EDX after washed only with acetone, ethanol, and distilled water (a); treated with step S (b); step S and P (c); step S, P, and A (d). The SEM image shows that micro-pore (500 nm in diameter) was formed by step S. The EDX and SEM image revealed that step A deposits fine particles of amorphous calcium phosphate. (e); 24 h after the immersion of PrA-treated PEEK in SBF, apatite was homogeneously formed.

used per experiment for each group, and every *in vitro* test was repeated at least three times to confirm the reproducibility. After incubation for the required period, each experiment was performed as below.

2.3.1. Cell adhesion on SEM

After 6-h culture, each substrate was washed with phosphate-buffered saline and fixed with 2.5% glutaraldehyde for 2 h. Then, the substrates were dehydrated in serial concentrations of ethanol (50%, 70%, 90%, 99%, 100%, and 100% [v/v]) for 10 min at each concentration. The substrates were soaked in 50% hexamethyldisilazane (HMDS) (Sigma-Aldrich) with 50% ethanol for 10 min, and then soaked in 100% HMDS for 20 min in sequence. All the surfaces of the PEEK plates were coated with platinum and then examined by SEM (S-4700; Hitachi Ltd, Tokyo, Japan).

2.3.2. Cell viability

Cell viability was evaluated by XTT assay, which utilizes cleavage, by metabolically active cells, of the yellow tetrazolium salt XTT to form an orange formazan dye. After 4-d culture, XTT labeling reagent (Roche Applied Science, USA) was added to each well. After incubation for 4 h, 150 μL of the medium was transferred to a 96-well plate and the amount of formazan product was quantified by absorbance at 450 nm using a microplate reader (iMark™ Microplate Absorbance Reader, BIO-RAD Laboratories, Hercules, California).

2.3.3. Alkaline phosphatase (ALP) activity at protein level

ALP activity was evaluated with p-nitrophenyl phosphate (pNPP) (Wako Pure Chemical Industries, Ltd., Osaka, Japan). After 7-d culture, the cells were washed with normal saline twice and lysed in 1% NONIDET NP-40 (Iwai Kagaku, Tokyo, Japan) by repeated pipetting. After 30-min incubation with 6.7 mM pNPP at 37 °C for 30 min (Wako Pure Chemical Industries, Ltd., Osaka, Japan), the optical density at 405 nm was measured, and ALP activities were calculated from a standard curve. The ALP levels were normalized to the total protein content and relative values were described.

2.3.4. Real-time quantitative PCR (RT-qPCR) analysis

After 7-d culture, the osteogenic differentiation-related genes (*Alp, Ocn, Opn*) and adhesion-related gene (*integrin-β1*) were quantified by RT-qPCR. RNA of the cells on each PEEK substrate was extracted with RNeasy Mini Kit (Qiagen, Hilden, Germany) and reverse transcribed into cDNA with ReverTra Ace qPCR RT Master Mix (TOYOBO, Japan). The cDNA samples were quantified using a LightCycler system (Roche) with THUNDERBIRD SYBR qPCR Mix (TOYOBO, Japan). The primer sequences used are listed in Table 1. The expression levels of osteogenic differentiation-related genes were evaluated and normalized to the internal housekeeping gene (*Gapdh*).

Table 1
Primer sequences of each gene in RT-qPCR analysis.

Gene	Forward (F) and Reverse (R) primer sequence (5′-3′)
Gapdh	F: TGTCCGTCGTGGATCTGAC
	R: CCTGCTTCACCACCTTCTTG
Alp	F: ACTCAGGGCAATGAGGTCAC
	R: CACCCGAGTGGTAGTCACAA
Ocn	F: AGACTCCGGCGCTACCTT
	R: CTCGTCACAAGCAGGGTTAAG
Opn	F: GGAGGAAACCAGCCAAGG
	R: TGCCAGAATCAGTCACTTTCAC
Integrin-β1	F: TTGGGATGATGTCGGGAC
	R: AATGTTTCAGTGCAGAGCC

2.4. In vivo study

2.4.1. Animals

The present study was approved by the Animal Research Committee, Graduate Scholl of Medicine, Kyoto University, Japan (Approval number; Med Kyo 17228 and 18259). A total of 33 male white rabbits weighing from 2.8 to 3.0 kg (15 weeks old) were used, and two legs from each were operated on. The rabbits were sacrificed at three time points, 4, 8, and 16 weeks after the operation, respectively (11 rabbits at each time point). At each time point, the legs of six rabbits (12 legs) were used for biomechanical tests and those from five rabbits (10 legs) were used for radiological and histological analysis. In each individual leg, either of the treatment type of PEEK substrate (group N or SPA) was implanted. Finally, for each time point and each treatment group, six implants were subjected to biomechanical tests and five implants were taken for radiological and histological analysis. Group SP was not tested in this study because preliminary experiments showed very poor bone-bonding, and evaluation of this group was stopped for animal welfare reasons.

2.4.2. Surgical procedure

Each PEEK substrate was implanted according to the methods our group previously reported [24]. Briefly, the rabbits were anesthetized with a gradual intravenous injection of pentobarbital sodium (40 mg/kg) followed by an inhalation of isoflurane and local injection of 1% lidocaine. A 4-cm longitudinal skin incision on the medial side of the tibia was made, and the fascia was incised. The periosteum was cut in an L-shape at the anterior verge of the medial collateral ligament, and then the tibial bone cortex was exposed. A 16 × 2 mm slit was made in the proximal metaphysis with a high-speed burr along the longitudinal axis of the tibia, and the slit was irrigated with saline. Either a group N or a group SPA PEEK substrate was implanted in the slit in a press-fit manner in one side of the tibial bone (Fig. 1A(b)), and the substrate from the other group was implanted in the other side. Thereafter, the fascia and the skin were sutured layer by layer. After the operation, the rabbits were housed and raised in a standard rabbit cage and given standard rabbit food and water. At 4, 8, and 16 weeks after the operation, the rabbits were sacrificed with 3 ml rapid intravenous injection of pentobarbital sodium. Segments of the tibial metaphysis bearing the PEEK substrate were cut and immersed in saline. For the biomechanical tests, bone and soft tissue formed outside the tibial bone were removed from both medial and lateral sides to evaluate the bone–PEEK bonding strength achieved within the tibial bone. For histological and radiological analysis, the specimens were immediately immersed in phosphate-buffered formalin.

2.4.3. Biomechanical testing

To evaluate bonding strength between PEEK substrate and tibial bone, the detachment test was applied within 5 h after sacrifice according to the protocol previously reported by Nakamura [24]. Vertical traction force was applied to the tibial bone at a cross-head speed of 35 mm/min using an Instron-type autograph (Model 1011; Aikoh Engineering Co. Ltd., Nagoya, Japan). In this apparatus, hooks held and pulled the anterior and posterior portion of the tibial bone divided by the PEEK substrate (Fig. 1A(c)). The detachment failure load was defined as the maximum force when the PEEK substrate was detached from the bone at any point. The failure load was taken as 0 N when the bone was detached by the weight of the hooks in the apparatus alone.

2.4.4. Radiological analysis using μ-CT

After harvesting the proximal segments of the tibia, each sample was evaluated using μ-CT scanning (SMX-100CT-SV-3; Shi-

madzu Corp., Kyoto, Japan) with a slice thickness of 0.05 mm under identical conditions. Three-dimensional CT images of each PEEK sample were reconstructed, and the newly-formed bone (NFB) mentioned below was calculated with VG studio MAX 2.2 (Volume Graphics GmbH, Heidelberg, Germany). Prior to evaluating the NFB around each PEEK substrate, a CT threshold value equating to that of the cortical bone was set, and this threshold was applied to all the samples. Second, a region of interest (designated ROI-1) which had the same or a higher CT value than the threshold was extracted. Then ROI-2 was defined as the space inside a sphere of radius 2.0 mm within the cancellous bone, the center of which was 10 mm distal to the proximal end of the tibia. Finally, the NFB was defined as the region included within both ROI-1 and ROI-2. The volume of NFB was measured and the proportion of NFB to ROI-2 (v/v) was calculated.

2.4.5. Histology

The bone specimens were first fixed in 10% phosphate-buffered formalin (pH 7.25) for 10 d, dehydrated in a series of ethanol concentrations (70%, 80%, 90%, 99%, 100%, and 100% [v/v]) for 1 d at each concentration, and then embedded in polyester resin. The specimens were cut into slices about 700 μm in width with a band saw (BS- 3000CP, EXACT cutting system; Exakt Apparatebau GmbH, Norderstedt, Germany) perpendicular to the tibial bone axis. Then, the sections were ground to a thickness of 80 μm using a grinding–sliding machine (Microgrinding MG-4000; Exakt Apparatebau GmbH) with continuous abrasive papers (#400, #800, #1200, #2000, and #4000). For light microscopy analysis, each ground section was stained with Stevenel's blue and van Gieson's picrofuchsin, by which calcified bone was stained bright red, non-calcified bone was stained green, and soft tissue was stained blue. Each stained sample was scrutinized using a transmitted light microscope (Eclipse 80i; Nikon, Tokyo, Japan) with digital camera attached (DS-55M-L1; Nikon, Tokyo, Japan). The direct contact between bone and PEEK substrate seen using light microscopy was quantified by measuring the bone–implant contact (BIC) ratio using 2-dimensional image processing software (Image J; National Institutes of Health, Bethesda, MA, USA). The BIC ratio was evaluated at three points: the proximal third, the middle third, and the distal third of each PEEK sample. The average value was then calculated. For SEM analysis, the ground sample was coated with platinum and examined by SEM (S-4700; Hitachi Ltd, Tokyo, Japan).

2.5. Statistical analysis

One-way analysis of variance (ANOVA) followed by Tukey's multiple comparison tests were used in *in vitro* analyses including XTT assay, ALP activity, and RT-qPCR among three groups (group N, SP, and SPA). Student's *t*-test was used for *in vivo* analysis for detachment tests (failure load) and BIC ratio between the two groups (group N and SPA). A P value < 0.05 was considered statistically significant. The statistical analysis was performed using JMP software (version 12.0.1, SAS Institute, Cary, NC, USA).

3. Results

3.1. Surface characteristics

3.1.1. XPS

The XPS profile of groups N, S, SP, and SPA are shown in Fig. 2A. In group S, there was a peak derived from S—O bonding in S2p. In group SP, a peak derived from O═C—O bonding was also found in C1s, and a peak derived from S—O was stronger compared with that in group S. In group SPA, both S—O bonding and O═C—O bonding were identified, and the presence of Ca and P was indicated in Ca2p and P2p. These results indicate that sulfo groups and carboxyl groups were introduced by step S and P respectively and that Ca and P were finally introduced by step A.

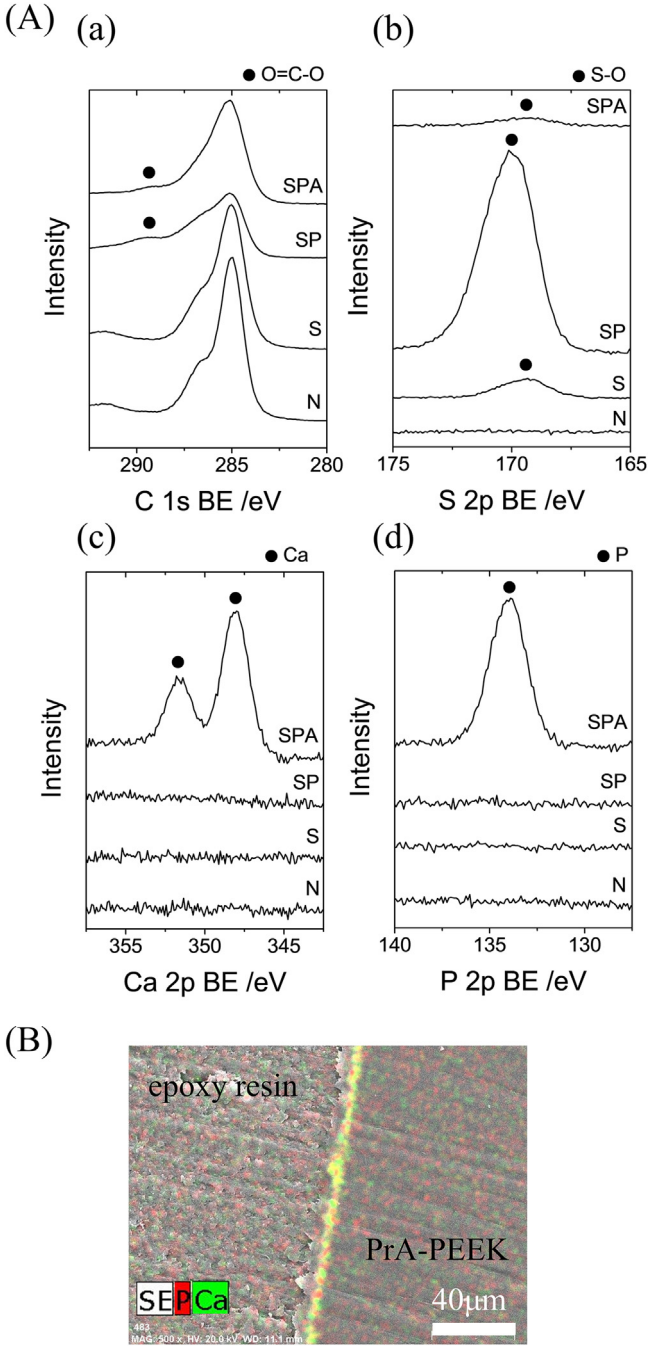

Fig. 2. (A): The XPS profile of groups N, S, SP, and SPA. (B) The PrA-PEEK substrate embedded in epoxy resin observed by SEM with EDX mapping.

3.1.2. Hydrophilicity, Ca/P ratio, and the thickness of PrA

The WCA of groups N, S, SP, and SPA were 86.9 ± 4.6°, 107.0 ± 2.5°, 16.5 ± 3.7°, and 7.4 ± 1.4°, respectively. The surface of PEEK substrate became hydrophobic by step S at the beginning, then hydrophilicity was given and increased by step P and A. Finally, the surface of group SPA showed super-hydrophilicity. In the SPA group, the estimated Ca/P ratio of PrA was 1.62 ± 0.15.

The SEM image with EDX mapping revealed that the thickness of PrA was less than 5 μm (Fig. 2B).

3.2. In vitro study

3.2.1. Cell adhesion visualized with SEM

Cell adhesion after 6-h incubation was observed by SEM (Fig. 3). In groups N and SPA, pseudopodia and spreading of cells were observed. In group SP, the cells remained spherical.

3.2.2. Cell viability

Viability of the seeded MC3T3-E1 cells after 4-d culture in α-MEM was evaluated by XTT assay (Fig. 4A). The mean relative cell viability and its standard deviation (SD) of groups N, SP, and SPA were 1.00 ± 0.18, 1.15 ± 0.06, and 1.63 ± 0.45, respectively. Cell viability of group SPA was significantly higher than that of groups N and SP ($p < 0.05$). There was no significant difference between groups N and SP.

3.2.3. ALP activity at protein level

ALP activity of the seeded MC3T3-E1 cells after 7-d culture on each substrate was assessed at protein level (Fig. 4B). The mean of relative ALP activity and its SD of groups N, SP, and SPA were 1.00 ± 0.35, 0.72 ± 0.12, and 0.27 ± 0.14, respectively. Contrary to expectations, ALP activity in group SPA was significantly lower than that of group N ($p < 0.05$). Although not statistically significant, ALP activity in group SPA tended to be lower than in group SP ($p = 0.053$). No statistical difference was found between group N and SP.

3.2.4. RT-qPCR

Relative gene expression levels of *Alp*, *Ocn*, *Opn,* and *integrin-β1*of MC3T3-E1 cells after 7-d culture was measured using RT-qPCR (Fig. 4C–F). The mean relative expression and its SD of these four genes in groups N, SP, and SPA was, respectively: *Alp*: 1.00 ± 0.38, 0.98 ± 0.13, and 0.25 ± 0.03; *Ocn*: 1.00 ± 051, 0.47 ± 0.22, and 0.41 ± 0.09; *Opn*: 1.00 ± 0.10, 1.15 ± 0.13, and 1.13 ± 0.27; *integrin-β1*: 1.00 ± 0.03, 0.62 ± 0.11, and 0.36 ± 0.06. As in ALP activity at protein level, expression of *Alp* in group SPA was significantly lower than that in group N and SP ($p < 0.01$). There was no significant difference of *Alp* expression between N and SP. As for *Ocn* and *Opn*, no significant differences were found between any of the groups. Expression of *integrin-β1* in group SPA was significantly lower than that in groups N and SP ($p < 0.01$). Moreover, *integrin-β1* expression in group SP was also significantly lower than that in group N ($p < 0.01$).

3.3. In vivo study

The surgical procedures were performed uneventfully in all the animals. No infection of the operation site or implant dislocation was observed during necropsy. No apparent adverse reactions, such as inflammation or foreign body reaction, were found on any of the implanted plates.

3.3.1. Biomechanical testing

Bonding strength between tibial bone and PEEK substrate was assessed by detachment testing (Fig. 5A). The mean failure loads and its SD for groups N and SPA were 1.0 ± 0.9 N and 12.2 ± 5.9 N at 4 weeks, 2.9 ± 4.9 N and 23.4 ± 13.2 N at 8 weeks, and 1.7 ± 3.1 N and 25.3 ± 9.5 N at 16 weeks, respectively. The failure loads for group SPA were significantly higher than for N at all time points ($p < 0.01$). The mean failure load for group SPA reached its plateau at 8 weeks and the bonding strength was maintained at 16 weeks.

3.3.2. New bone formation as visualized by μ-CT

Representative axial images of μ-CT data are shown in Fig. 5B. New bone formation seemed to take place from the surface of the tibial bone in both N and SPA groups. However, NFB in group N remained somewhat separated from the PEEK substrate while NFB in the SPA group was formed at the surface of the PEEK sub-

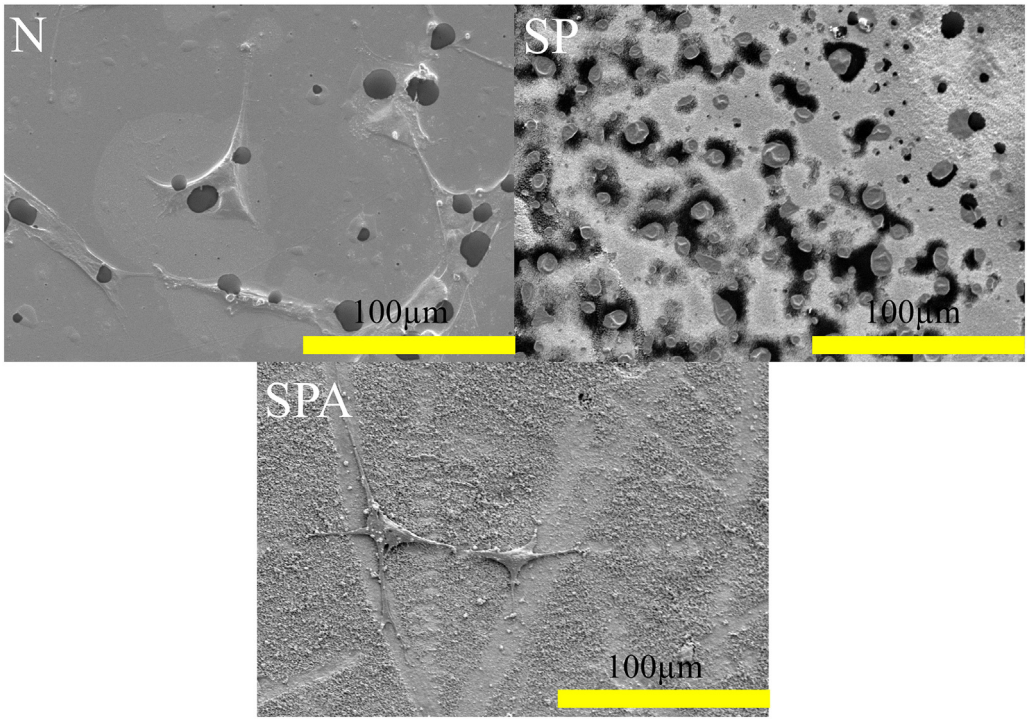

Fig. 3. Cell attachment on each PEEK substrate after 6-h incubation observed by SEM.

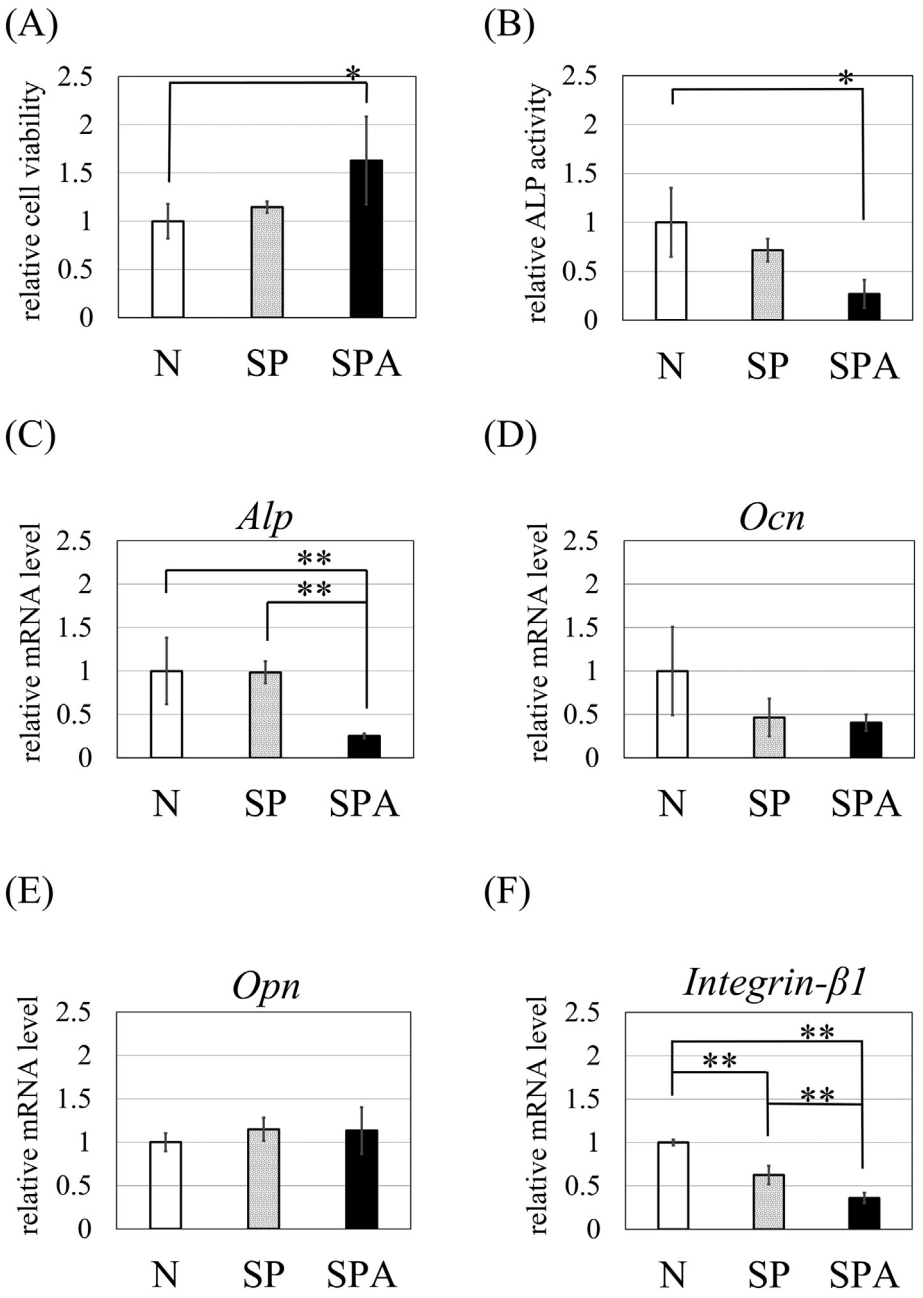

Fig. 4. Cell viability shown by XTT assay at 4-d incubation (A), ALP activity at 7-d incubation (B), and gene expression levels at 7-d incubation using RT-qPCR (C–F). The symbol "*" indicates $p < 0.05$ and "**" indicates $p < 0.01$ by One-way analysis of variance (ANOVA) followed by Tukey's multiple comparison tests.

strate at all time points. The proportion of NFB volume to the defined ROI was also calculated from μ-CT scans (Fig. 5C). The mean values and its SD for NFB volume in groups N and SPA were 1.6 ± 1.2% and 9.0 ± 2.4% at 4 weeks, 1.5 ± 1.4% and 5.4 ± 4.6% at 8 weeks, and 0.4 ± 0.2% and 6.2 ± 4.3% at 16 weeks, respectively. NFB volume in group SPA was greater than that in group N at 4 weeks ($p < 0.01$) and 16 weeks ($p < 0.05$), though there was no significant difference between the two groups at 8 weeks.

3.3.3. Histology and histomorphometry

Representative SEM images of the interface between the PEEK substrate and tibial bone are shown in Fig. 6A. In group N, the interface showed detachments in many places while the interface was more attached in group SPA. Direct contact between tibial bone and the PEEK substrate was scrutinized by light microscopy. Representative histological specimens are shown in Fig. 6B. At 4 weeks, soft tissue was seen penetrating between the PEEK substrate and tibial bone over most areas of the PEEK surface in group N, while immature bone in direct contact with the PEEK substrate had formed in group SPA. At 8 weeks, new bone also started forming in group N, although most of the NFB was not in direct contact with the PEEK substrate; at this point, NFB in group SPA was beginning to mature and was in direct contact with the PEEK substrate. This difference between the two groups was also present at 16 weeks. Direct contact between the PEEK substrate and tibial bone was quantified by measuring BIC ratio (Fig. 6C). The mean value of BIC ratio of group N and SPA were 8.6 ± 2.9% and 51.5 ± 10.0% at 4 weeks, 20.3 ± 3.3% and 53.5 ± 9.1% at 8 weeks, and 23.2 ± 6.3% and 53.9 ± 3.4% at 16 weeks, respectively. The BIC ratio in group N gradually increased with time, but remained

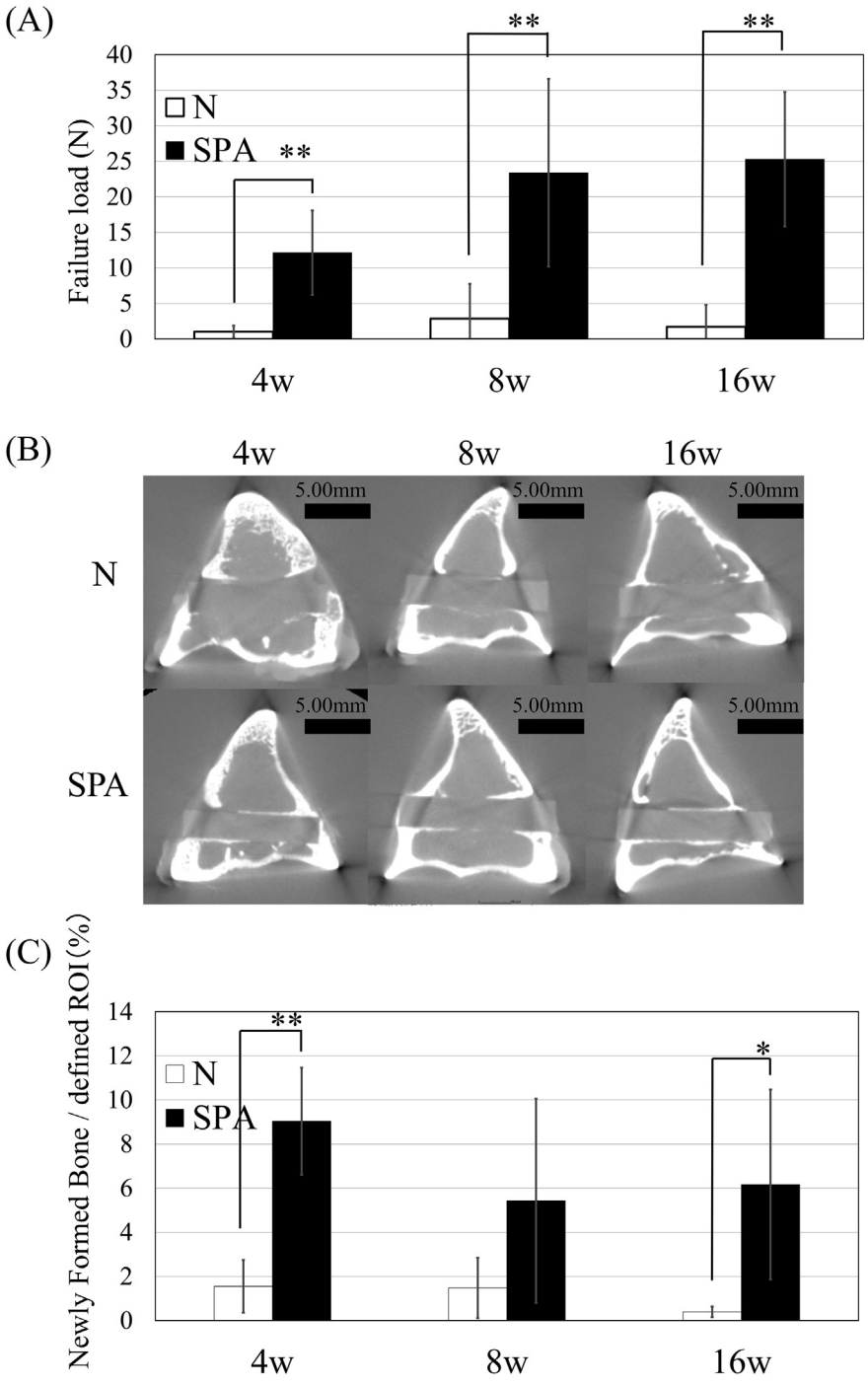

Fig. 5. (A): The results of the detachment test. (B): Representative μ-CT images of the implanted PEEK. (C): The quantification of newly-formed bone (NFB) around the PEEK substrates in the same region of interest on μ-CT. The symbol "*" indicates $p < 0.05$ and "**" indicates $p < 0.01$ by Student's *t*-test.

low, even at 16 weeks. In contrast, the BIC ratio in group SPA was significantly higher than in group N throughout the experiment ($p < 0.01$). The BIC ratio in group SPA reached its plateau as early as 4 weeks and was maintained at 16 weeks.

4. Discussion

In our previous reports, apatite was homogeneously formed on PrA-treated PEEK (PrA-PEEK) in SBF within 24 h, and we noted that if any one of the three processing steps (S, P, or A) was omitted the apatite formed on the PEEK substrate was either less in volume or more spathic in nature compared with group SPA PEEK [20]. Results *in vivo* in the present study for the detachment test, BIC ratio (histology), and NFB (μ-CT) revealed that PrA treatment produced excellent bone-bonding properties and osteo-conductivity on the PEEK surface. *In vitro* results obtained from the XTT assay revealed that SPA treatment confers no cytotoxicity. Contrary to expectations, however, expression of adhesion- and differentiation-related genes (*integrin-β1* and *Alp*) of pre-osteoblast cells on PrA-PEEK was suppressed.

There are several advantages to the PrA treatment described here. First of all, bone-bonding of PrA-PEEK *in vivo* was accom-

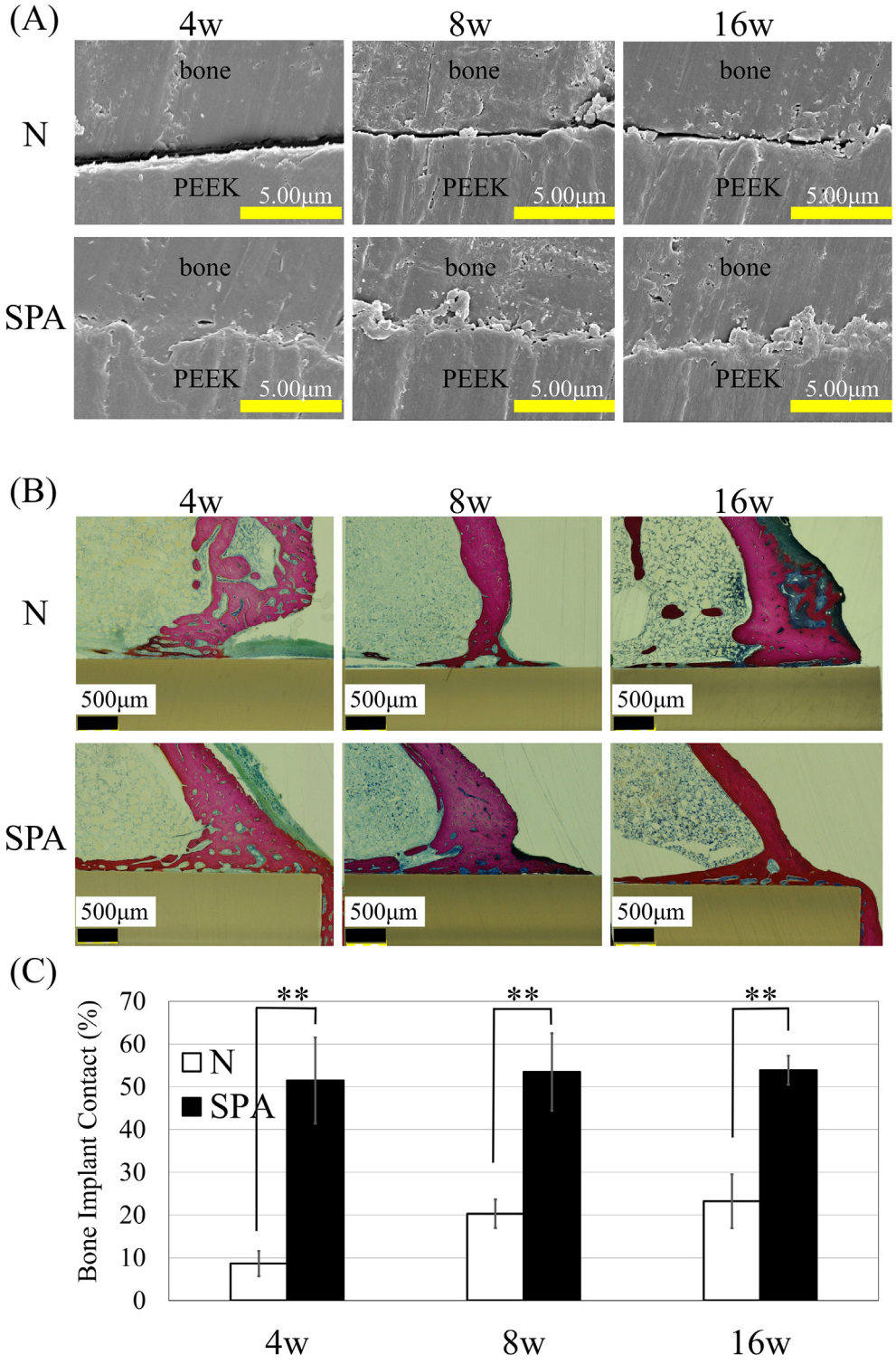

Fig. 6. (A): Representative SEM images of the interface between PEEK substrate and tibial bone. (B): Representative histology samples of the implanted PEEK substrate stained with Stevenel's blue and van Gieson's picrofuchsin. (C): Bone–implant contact (%) (BIC) of each group of PEEK. The symbol "**" indicates $p < 0.01$ by Student's *t*-test. (For interpretation of the references to color in this figure legend, the reader is referred to the web version of this article.)

plished relatively early after implantation, and was maintained for a comparatively long period. In the present study, Ca/P ratio of our PrA (Ca/P = 1.62) was a slightly higher than the past reported value of ACP (Ca/P = 1.50) [25], which indicated that PrA was Ca-rich ACP. Nagano et al. evaluated *in vivo* bone-bonding property and degradation behavior of ACP and crystalline hydroxyapatite; they concluded that hydroxyapatite is preferable for coating longevity while ACP is advantageous for initial fixation for porous materials [26]. Consistent with this report, ACP deposited on PrA-PEEK conveyed bioactivity early after implantation. Second, the maximum temperature used in the PrA treatment (70 °C for 24 h in step A) is significantly below the melting point (335 °C) and the glass transition point (143 °C) of PEEK [3]. Therefore, any heat-associated damage to the PEEK substrate may be minimized and its surface

Table 2
Results from previous reports on water contact angle (WCA), and its effect *in vivo* and *in vitro* on bioactive PEEK. The symbols "↑," "→," and "↓" indicate "activated," "levelled," and "suppressed," respectively.

Author	Treatment	WCA(°)	*in vivo* effect	*in vitro* effect		
			Bone-bonding property (animals)	Cell adhesion (observation method/cell line)	Cell compatibility (method/cell line)	Cell differentiation (method/cell line)
P. Johansson et al. [33]	Nano-crystalline hydroxyapatite coating	88 ± 2.7	↑ (rabbits)	N/A	N/A	N/A
K. Gan et al. [16]	Nitrogen plasma immersion ion implantation	17.74–20.67	N/A	↑ (SEM/MG-63)	↑ (MTT assay/MG-63)	↑ (ALP activity assay/MG-63)
C.M. Han et al. [34]	electron beam deposition of titanium	54 ± 2.4	↑ (rabbits)	↑ (SEM/MC3T3-E1)	↑ (MTS method/MC3T3-E1)	↑ (ALP activity assay/ MC3T3-E1)
X. Liu et al. [35]	Polystyrene sulfonate (PSS) and polyallylamine hydrochloride (PAH) multilayers	21.7–39.7	↑ (rabbits)	↑ (SEM/rat bone marrow stromal cell)	↑ (CCK-8 kit/rat bone marrow stromal cell)	↑ (ALP activity assay/rat bone marrow stromal cell)
T. Shimizu et al. [18]	Sol–gel-derived TiO_2 coating	18.3 (O_2 plasma)–41.0 (sandblast)	↑ (rabbits)	↑ (phalloidin stained/bone mesenchymal stem cell of rabbit)	↑ (XTT assay/bone mesenchymal stem cell of rabbit)	↑ (ALP activity assay/bone mesenchymal stem cell of rabbit)
Y. Zhao et al. [36]	Three-dimensional porous and nanostructured network by H_2SO_4	88–92	↑ (rats)	↑ (phalloidin stained/ MC3T3-E1)	↑ (MTT assay/MC3T3-E1)	↑ (gene expression of *Alp*/ MC3T3-E1)
Rui Ma et al. [37]	Nano-hydroxyapatite/ polyetherether-ketone biocomposite	51	N/A	↑ (phalloidin stained/ MC3T3-E1)	↑ (cell counting kit-8 assay/MC3T3-E1)	↑ (ALP activity assay/ MC3T3-E1)
Our group	PrA-PEEK	7.4 ± 1.4	↑ (rabbits)	→ (SEM/MC3T3-E1)	↑ (XTT assay/MC3T3-E1)	↓ (ALP activity assay/ MC3T3-E1)

micro-structure is comparatively easy to control. Third, the micropores formed in step S are relatively fine (500 nm in diameter) and the depth of the pore layer can be maintained to <5 μm by limiting the immersion time in H_2SO_4 in step S to only 4 s. Thus, ACP rich in chemical reactivity is deposited, the specific surface area of the PEEK can be increased, adhesion to apatite or bone tissue is improved, while changes in surface properties are minimized. We speculate that it is this fine structure that is responsible for the excellent *in vivo* bone-bonding properties demonstrated in this study. Finally, PrA treatment does not need special chemicals or apparatus other than H_2SO_4 and glow-discharge equipment. Overall, PrA treatment can affordably yield a valuable medical material in an age when medical budgets are very tight.

Unexpected results from the *in vitro* tests raise some crucial questions. The first is the possibility that residual sulfo groups in PrA can suppress pre-osteoblast differentiation. Miyazaki et al. reported that sulfo groups on carbon-PEEK could accelerate apatite formation in SBF immersion test [27]. On the other hand, Ouyang et al. developed sulfonated PEEK, which had a three dimensional network by immersion in H_2SO_4 and evaluated the effect of residual sulfo-compounds on osteoblast [28]. Their study showed that PEEK with small sulfur concentration accelerated proliferation and differentiation of rat bone mesenchymal stem cells, but the PEEK with high sulfur concentration suppressed them. In PrA-PEEK, EDX did not detect sulfur content, but XPS did. Therefore, even though the amount of residual sulfo groups may be small in PrA-PEEK, they could suppress differentiation of pre-osteoblast.

The second is that crystallinity of calcium phosphate may influence differentiation of pre-osteoblast. Even though ACP was reported to accelerate cell adhesion and osteogenic differentiation [29], it is still debatable. In fact, Hu et al. reported that crystalline hydroxyapatite was better than ACP for osteogenic differentiation when the factor of the size of nanoparticles was removed [30]. One feature peculiar to ACP is that ACP autonomously changes into hydroxyapatite in aqueous media [29]. We speculate that this richness in chemical reactivity may not necessarily have a positive effect on the differentiation of pre-osteoblast. Taking into account the excellent results of SBF test in our past study, apatite formation on our PrA-PEEK seemed to depend not on direct activation of pre-osteoblasts but on an inorganic chemical reaction, such as $10Ca^{2+} + 6PO_4^{3-} + 2OH^- \leftrightarrow Ca_{10}(PO_4)_6(OH)_2$ at a very early stage.

The third is that the hydrophilic nature of the PEEK substrate may have different influences at cell and organism levels. Conferring hydrophilicity on PEEK by plasma treatment is a frequently-used technique for promotion of bioactivity [14,31]. At the cell level, wettability, along with topography, charge, pore size, and bioactivity, is regarded as a determining factor for cell adhesion [32]. When compared with bioactive PEEK reported previously (Table 2) [16,18,33–37], our PrA-PEEK showed super-hydrophilicity in terms of WCA (WCA = 7.4 ± 1.4°). As for cell response, Tamada et al. investigated L cell attachment on various kinds of polymer surface and the relationship between cell attachment and hydrophilicity using WCA [38] and revealed that L cells preferentially adhere to moderately wettable substrates having a WCA of 60°–80° in the medium regardless of the presence of serum. Van Wachem et al. evaluated the adhesion of human endothelial cells in serum-containing culture medium on methacrylate polymer surfaces having varying wettability and revealed that cell adhesion to the polymer was optimal on moderately wettable polymer (at a WCA of around 39°) [39]. Therefore, super-hydrophilicity may explain suppressed gene expression of cell adhesion-related genes such as *integrin-β1*. Moreover, considering that integrin plays a leading role not only in cell attachment but also as a trigger of the differentiation-related signaling cascade

[32] (including Ras-MAPK/ERK1/2 [40], Src/FAK-p130Cas-Rho GTPases [41], ERK1/2-Bcl-xL/Bcl2 [42], and PI3K-Akt-mTOR [43]), expression of differentiation-related genes (such as *Alp*) may be suppressed owing to the suppression of integrin caused by super-hydrophilicity. To maximize the bioactivity of PEEK, we should further investigate optimal hydrophilicity for PrA-PEEK.

Finally, *in vitro* experiments as a predictor of *in vivo* bioactivity should be reconsidered. The prediction of *in vivo* bioactivity without using animals has become increasingly important. Intuitively, the activity of pre-osteoblasts on the PEEK substrate should reflect *in vivo* behavior better than the SBF test. However, in evaluating PrA-PEEK, the opposite result was observed in the present study. Therefore, the prediction of *in vivo* bioactivity should be done in combination with multiple *in vitro* tests.

There were some limitations in the present study. First, only groups N and SPA were tested in *in vivo* studies. Therefore, the effect of change in topology or hydrophilicity on *in vivo* bioactivity were not evaluated. Second, only the single conditions of immersion time in H_2SO_4 and the voltage and exposure time in glow discharge were evaluated. They may be the critical factors that maximize the bioactivity of our PrA-PEEK. Third, the adhesion strength between PrA and PEEK substrate was not evaluated because of technical problems. This data may be essential for clinical application as orthopedic implants. Finally, we were also unable to directly evaluate the activity of pre-osteoblast *in vivo* due to technical difficulties, which is the key in understanding the discrepancy in the present results between *in vivo* and *in vitro*. All these issues that have been discussed will be the focus of future research.

5. Conclusion

Our PrA treatment on PEEK substrate succeeded in giving fast and long-lasting bone-bonding strength and promoting new bone formation *in vivo* without the need for a high-temperature procedure, although the treatment did not accelerate pre-osteoblast cell adhesion or differentiation on the PEEK substrate. A balancing act of exposure times in steps S and P is needed to maximize the bioactivity of PrA-PEEK.

Acknowledgement

We greatly appreciate the technical support of Mr. Kohda and Ms. Furuta for the SEM studies. Investigation of The PEEK sample preparation process was partly supported by JSPS KAKENHI (16K16401) and Kyoto University Research Development Program "Ishizue".

Disclosures

This work received grants from Eli Lilly Japan K.K. Two authors (S.F. and K.G.) were financially supported by KYOCERA, Kyoto, Japan.

References

[1] S.M. Kurtz, J.N. Devine, PEEK biomaterials in trauma, orthopedic, and spinal implants, Biomaterials 28 (2007) 4845–4869, https://doi.org/10.1016/j.biomaterials.2007.07.013.

[2] S. Seaman, P. Kerezoudis, M. Bydon, J.C. Torner, P.W. Hitchon, Titanium vs. polyetheretherketone (PEEK) interbody fusion: meta-analysis and review of the literature, J. Clin. Neurosci. 44 (2017) 23–29, https://doi.org/10.1016/j.jocn.2017.06.062.

[3] I.V. Panayotov, V. Orti, F. Cuisinier, J. Yachouh, Polyetheretherketone (PEEK) for medical applications, J. Mater. Sci. Mater. Med. 27 (2016) 118, https://doi.org/10.1007/s10856-016-5731-4.

[4] S.B. Park, C.K. Chung, Strategies of spinal fusion on osteoporotic spine, J. Korean Neurosurg. Soc. 49 (2011) 317–322, https://doi.org/10.3340/jkns.2011.49.6.317.

[5] D. Almasi, N. Iqbal, M. Sadeghi, I. Sudin, M.R. Abdul Kadir, T. Kamarul, Preparation methods for improving PEEK's bioactivity for orthopedic and dental application: a review, Int. J. Biomater. 2016 (2016), https://doi.org/10.1155/2016/8202653.

[6] M.S. Abu Bakar, M.H.W. Cheng, S.M. Tang, S.C. Yu, K. Liao, C.T. Tan, K.A. Khor, P. Cheang, Tensile properties, tension-tension fatigue and biological response of polyetheretherketone-hydroxyapatite composites for load-bearing orthopedic implants, Biomaterials 24 (2003) 2245–2250, https://doi.org/10.1016/S0142-9612(03)00028-0.

[7] J.P. Fan, C.P. Tsui, C.Y. Tang, C.L. Chow, Influence of interphase layer on the overall elasto-plastic behaviors of HA/PEEK biocomposite, Biomaterials 25 (2004) 5363–5373, https://doi.org/10.1016/j.biomaterials.2003.12.050.

[8] L. Wang, S. He, X. Wu, S. Liang, Z. Mu, J. Wei, F. Deng, Y. Deng, S. Wei, Polyetheretherketone/nano-fluorohydroxyapatite composite with antimicrobial activity and osseointegration properties, Biomaterials 35 (2014) 6758–6775, https://doi.org/10.1016/j.biomaterials.2014.04.085.

[9] K.L. Wong, C.T. Wong, W.C. Liu, H.B. Pan, M.K. Fong, W.M. Lam, W.L. Cheung, W. M. Tang, K.Y. Chiu, K.D.K. Luk, W.W. Lu, Mechanical properties and in vitro response of strontium-containing hydroxyapatite/polyetheretherketone composites, Biomaterials 30 (2009) 3810–3817, https://doi.org/10.1016/j.biomaterials.2009.04.016.

[10] C. Von Wilmonsky, R. Lutz, U. Meisel, S. Srour, S. Rupprecht, T. Toyoshima, E. Nkenke, K.A. Schlegel, D. Pohle, H. Munstedt, T. Rechtenwald, M. Schmidt, In vivo evaluation of β-TCP containing 3D laser sintered poly(ether ether ketone) composites in pigs, J. Bioact. Compat. Polym. 24 (2009) 169–184, https://doi.org/10.1177/0883911508101149.

[11] X. Wu, X. Liu, J. Wei, J. Ma, F. Deng, S. Wei, Nano-TiO2/PEEK bioactive composite as a bone substitute material: in vitro and in vivo studies, Int. J. Nanomed. 7 (2012) 1215–1225, https://doi.org/10.2147/IJN.S28101.

[12] I.Y. Kim, A. Sugino, K. Kikuta, C. Ohtsuki, S.B. Cho, Bioactive composites consisting of PEEK and calcium silicate powders, J. Biomater. Appl. 24 (2009) 105–118, https://doi.org/10.1177/0885328208094557.

[13] J. Marchand-brynaert, G. Pantano, O. Noiset, Surface fluorination of PEEK film by selective wet-chemistry, Polymer (Guildf) 38 (1997) 1387–1394, https://doi.org/10.1016/S0032-3861(96)00661-1.

[14] J. Comyn, L. Mascia, G. Xiao, B.M. Parker, Plasma-treatment of polyetheretherketone (PEEK) for adhesive bonding, Int. J. Adhes. Adhes. 16 (1996) 97–104, https://doi.org/10.1016/0143-7496(96)89798-3.

[15] Y. Zhao, H.M. Wong, S.C. Lui, E.Y.W. Chong, G. Wu, X. Zhao, C. Wang, H. Pan, K. M.C. Cheung, S. Wu, P.K. Chu, K.W.K. Yeung, Plasma surface functionalized polyetheretherketone for enhanced osseo-integration at bone-implant interface, ACS Appl. Mater. Interfaces 8 (2016) 3901–3911, https://doi.org/10.1021/acsami.5b10881.

[16] K. Gan, H. Liu, L. Jiang, X. Liu, X. Song, D. Niu, T. Chen, C. Liu, Bioactivity and antibacterial effect of nitrogen plasma immersion ion implantation on polyetheretherketone, Dent. Mater. 32 (2016) e263–e274, https://doi.org/10.1016/j.dental.2016.08.215.

[17] S. Barkarmo, A. Wennerberg, M. Hoffman, P. Kjellin, K. Breding, P. Handa, V. Stenport, Nano-hydroxyapatite-coated PEEK implants: a pilot study in rabbit bone, J. Biomed. Mater. Res. - Part A. 101 A (2013) 465–471, https://doi.org/10.1002/jbm.a.34358.

[18] T. Shimizu, S. Fujibayashi, S. Yamaguchi, K. Yamamoto, B. Otsuki, M. Takemoto, M. Tsukanaka, T. Kizuki, T. Matsushita, T. Kokubo, S. Matsuda, Bioactivity of sol-gel-derived TiO_2 coating on polyetheretherketone: in vitro and in vivo studies, Acta Biomater. 35 (2016) 305–317, https://doi.org/10.1016/j.actbio.2016.02.007.

[19] J. Wu, L. Li, C. Fu, F. Yang, Z. Jiao, X. Shi, Y. Ito, Z. Wang, Q. Liu, P. Zhang, Microporous polyetheretherketone implants decorated with BMP-2 via phosphorylated gelatin coating for enhancing cell adhesion and osteogenic differentiation, Colloids Surf. B Biointerfaces 169 (2018) 233–241, https://doi.org/10.1016/j.colsurfb.2018.05.027.

[20] T. Yabutsuka, K. Fukushima, T. Hiruta, S. Takai, T. Yao, Effect of pores formation process and oxygen plasma treatment to hydroxyapatite formation on bioactive PEEK prepared by incorporation of precursor of apatite, Mater. Sci. Eng. C 81 (2017) 349–358, https://doi.org/10.1016/j.msec.2017.07.017.

[21] Implants for Surgery: In Vitro Evaluation for Apatite- Forming Ability of Implant Materials (ISO 23317:2014, IDT), Int. Organ. Stand. (2014). https://books.google.com/books?id=zOtNnwEACAAJ.

[22] T. Kokubo, H. Takadama, How useful is SBF in predicting in vivo bone bioactivity?, Biomaterials 27 (2006) 2907–2915, https://doiorg/10.1016/j.biomaterials.2006.01.017.

[23] T. Yabutsuka, T. Hiruta, S. Takai, T. Yao, Changes in surface condition during fabrication process of bioactive apatite nuclei incorporated PEEK, Key Eng. Mater. 782 (2018) 182–188.

[24] T. Nakamura, T. Yamamuro, S. Higashi, T. Kokubo, S. Itoo, A new glass-ceramic for bone replacement: evaluation of its bonding to bone tissue, J. Biomed. Mater. Res. 19 (1985) 685–698, https://doi.org/10.1002/jbm.820190608.

[25] O. Suzuki, M. Nakamura, Y. Miyasaka, M. Kagayama, M. Sakurai, Bone formation on synthetic precursors of hydroxyapatite, Tohoku J. Exp. Med. 164 (1991) 37–50, https://doi.org/10.1620/tjem.164.37.

[26] M. Nagano, T. Nakamura, T. Kokubo, M. Tanahashi, M. Ogawa, Differences of bone bonding ability and degradation behaviour in vivo between amorphous

calcium phosphate and highly crystalline hydroxyapatite coating, Biomaterials 17 (1996) 1771–1777, https://doi.org/10.1016/0142-9612(95)00357-6.
[27] T. Miyazaki, C. Matsunami, Y. Shirosaki, Bioactive carbon–PEEK composites prepared by chemical surface treatment, Mater. Sci. Eng. C 70 (2017) 71–75, https://doi.org/10.1016/j.msec.2016.08.058.
[28] L. Ouyang, Y. Qiao, P.K. Chu, X. Liu, G. Jin, X. Zhang, Y. Zhao, J. Li, C. Ning, T. Lu, Influence of sulfur content on bone formation and antibacterial ability of sulfonated PEEK, Biomaterials 83 (2016) 115–126, https://doi.org/10.1016/j.biomaterials.2016.01.017.
[29] J. Zhao, Y. Liu, W. Bin Sun, H. Zhang, Amorphous calcium phosphate and its application in dentistry, Chem. Cent. J. 5 (2011) 40, https://doi.org/10.1186/1752-153X-5-40.
[30] Q. Hu, Z. Tan, Y. Liu, J. Tao, Y. Cai, M. Zhang, H. Pan, X. Xu, R. Tang, Effect of crystallinity of calcium phosphate nanoparticles on adhesion, proliferation, and differentiation of bone marrow mesenchymal stem cells, J. Mater. Chem. 17 (2007) 4690–4698, https://doi.org/10.1039/b710936a.
[31] D. Briem, S. Strametz, K. Schröoder, N.M. Meenen, W. Lehmann, W. Linhart, A. Ohl, J.M. Rueger, Response of primary fibroblasts and osteoblasts to plasma treated polyetheretherketone (PEEK) surfaces, J. Mater. Sci. Mater. Med. 16 (2005) 671–677, https://doi.org/10.1007/s10856-005-2539-z.
[32] S. Chen, Y. Guo, R. Liu, S. Wu, J. Fang, B. Huang, Z. Li, Z. Chen, Z. Chen, Tuning surface properties of bone biomaterials to manipulate osteoblastic cell adhesion and the signaling pathways for the enhancement of early osseointegration, Colloids Surf. B Biointerfaces 164 (2018) 58–69, https://doi.org/10.1016/j.colsurfb.2018.01.022.
[33] P. Johansson, R. Jimbo, P. Kjellin, F. Currie, B.R. Chrcanovic, A. Wennerberg, Biomechanical evaluation and surface characterization of a nano-modified surface on PEEK implants: a study in the rabbit tibia, Int. J. Nanomed. 9 (2014) 3903–3911, https://doi.org/10.2147/IJN.S60387.
[34] C.M. Han, E.J. Lee, H.E. Kim, Y.H. Koh, K.N. Kim, Y. Ha, S.U. Kuh, The electron beam deposition of titanium on polyetheretherketone (PEEK) and the resulting enhanced biological properties, Biomaterials 31 (2010) 3465–3470, https://doi.org/10.1016/j.biomaterials.2009.12.030.
[35] X. Liu, F. Han, P. Zhao, C. Lin, X. Wen, X. Ye, Layer-by-layer self-assembled multilayers on PEEK implants improve osseointegration in an osteoporosis rabbit model, Nanomed. Nanotechnol. Biol. Med. 13 (2017) 1423–1433, https://doi.org/10.1016/j.nano.2017.01.011.
[36] Y. Zhao, H.M. Wong, W. Wang, P. Li, Z. Xu, E.Y.W. Chong, C.H. Yan, K.W.K. Yeung, P.K. Chu, Cytocompatibility, osseointegration, and bioactivity of three-dimensional porous and nanostructured network on polyetheretherketone, Biomaterials 34 (2013) 9264–9277, https://doi.org/10.1016/j.biomaterials.2013.08.071.
[37] R. Ma, S. Tang, H. Tan, W. Lin, Y. Wang, J. Wei, L. Zhao, T. Tang, Preparation, characterization, and in vitro osteoblast functions of a nano-hydroxyapatite/polyetheretherketone biocomposite as orthopedic implant material, Int. J. Nanomed. 9 (2014) 3949–3961, https://doi.org/10.2147/IJN.S67358.
[38] Y. Tamada, Y. Ikada, Effect of preadsorbed proteins on cell adhesion to polymer surfaces, J. Colloid Interface Sci. 155 (1993) 334–339, https://doi.org/10.1006/jcis.1993.1044.
[39] P.B. van Wachem, A.H. Hogt, T. Beugeling, J. Feijen, A. Bantjes, J.P. Detmers, W. G. van Aken, Adhesion of cultured human endothelial cells onto methacrylate polymers with varying surface wettability and charge, Biomaterials 8 (1987) 323–328, https://doi.org/10.1016/0142-9612(87)90001-9.
[40] T. Jiang, L. Guo, S. Ni, Y. Zhao, Upregulation of cell proliferation via Shc and ERK1/2 MAPK signaling in SaOS-2 osteoblasts grown on magnesium alloy surface coating with tricalcium phosphate, J. Mater. Sci. Mater. Med. 26 (2015) 1–9, https://doi.org/10.1007/s10856-015-5479-2.
[41] K. Kaneko, M. Ito, Y. Naoe, A. Lacy-Hulbert, K. Ikeda, Integrin αv in the mechanical response of osteoblast lineage cells, Biochem. Biophys. Res. Commun. 447 (2014) 352–357, https://doi.org/10.1016/j.bbrc.2014.04.006.
[42] M. Niit, V. Hoskin, E. Carefoot, M. Geletu, R. Arulanandam, B. Elliott, L. Raptis, Cell-cell and cell-matrix adhesion in survival and metastasis: Stat3 versus Akt, Biomol. Concepts 6 (2015) 383–399, https://doi.org/10.1515/bmc-2015-0022.
[43] A. Santos, A.D. Bakker, B. Zandieh-Doulabi, J.M.A. de Blieck-Hogervorst, J. Klein-Nulend, Early activation of the β-catenin pathway in osteocytes is mediated by nitric oxide, phosphatidyl inositol-3 kinase/Akt, and focal adhesion kinase, Biochem. Biophys. Res. Commun. 391 (2010) 364–369, https://doi.org/10.1016/j.bbrc.2009.11.064.